JOURNAL OF MATERIALS SCIENCE **40** (2005) 6187–6193

Effect of variable radius on the initial creep rate of ceramic fibres

IAN J. DAVIES
Department of Mechanical Engineering, Curtin University of Technology, GPO Box U1987, Perth, WA 6845, Australia
E-mail: I.Davies@curtin.edu.au

Published online: 8 September 2005

The effect of variable fibre radius on the initial creep rate, $\dot{\varepsilon}^*$, of monofilament ceramic fibres was investigated using a numerical integration method. The following parameters were studied: (i) radius variation geometry, (ii) creep stress exponent, n, (iii) fractional radius variation, r_v, and (iv) fraction, m, of the characteristic radius variation wavelength, λ; the ranges of n ($0 < n < 3$) and r_v ($0 < r_v < 0.5$) were chosen to be similar to those for current ceramic fibres based on the silicon carbide (SiC) system. Values of $\dot{\varepsilon}^*$ were found to be consistently greater compared to those for a constant radius fibre with an equivalent mean radius and increased with both n and r_v. The main result of this work was a recommendation for creep testing of monofilament ceramic fibres to be limited to certain radius variation geometries and gauge lengths.

1. Introduction

Ceramic matrix composites (CMCs) have shown great promise with regards to their use as high-temperature (e.g., >1000 °C) structural materials in space and aerospace applications [1]. One important property of CMCs under these conditions is their resistance to creep, i.e., time-dependent deformation at a stress below that required for monotonic rupture. The creep of CMCs is known to depend on factors such as the creep rate, $\dot{\varepsilon}$, of the fibre and matrix components together with the fibre/matrix interface shear strength, τ [2]. For many applications the creep response will be dominated by a "steady-state" regime which is characterised by the following relationship [3]:

$$\dot{\varepsilon} = A\sigma^n e^{-\left(\frac{Q}{RT}\right)} \tag{1}$$

where A is an empirical constant, σ is the applied stress, n is the stress exponent, Q is the activation energy, R is the gas constant, and T is the absolute temperature. Values of n for fibres based on the silicon carbide (SiC) system have been presented in Table I with a range of $0.97 < n < 3.3$ being noted for the test conditions encountered [4–7]. It should be noted that the gauge length values shown in Table I refer to the length of fibre over which the creep rate was measured (and usually deduced from the temperature profile along the fibre length), rather than the actual length of fibre subject to stress.

One potential issue regarding the experimental determination of $\dot{\varepsilon}$ in ceramic fibres concerns the uniformity of the fibre radius, r, along its length. For a fibre of constant circular cross-section the value of σ in Equation (1) can be simply expressed as $F/(\pi r^2)$, where F is the creep load applied at the fibre ends. However, in practice there is always some degree of variation in r along the fibre length and thus the value of σ is generally replaced with $F/(\pi r_o^2)$, where r_o is the mean radius and is typically obtained by averaging several radius measurements along the fibre length using scanning electron microscopy. One issue regarding the use of r_o is that a cursory examination of Equation (1) indicates that any variation in radius along the fibre length will result in $\dot{\varepsilon}$ being overestimated when compared to a fibre of constant radius, r_o, with the error in $\dot{\varepsilon}$ being a function of n, the magnitude of radius variation, Δr, and the geometry of the radius variation along the fibre length. The measured value of $\dot{\varepsilon}$ can therefore be thought to comprise of a (fibre radius) geometry component superimposed onto the intrinsic material-related value expected for a fibre of constant radius, r_o. Whilst some researchers [6, 7] have explicitly stated that ceramic fibre creep data was only collected for those portions of fibres where the radius was essentially constant, other researchers make no mention of this point and it thus should be assumed that at least some of the published ceramic fibre creep data relates to fibres with significant variations in radius along the test gauge length.

The topic of radius variation in ceramic fibres and its effect on properties of the fibres and resulting composites has been the subject of recent research [8–15] with several investigations having indicated that the radius of many SiC-based fibres varies along the fibre length with a fractional radius variation, $r_v = \Delta r/r_o$, in the

0022-2461
DOI: 10.1007/s10853-005-3158-2

TABLE I Values of creep stress exponent for ceramic fibres based on the silicon carbide system [4–7]

Fibre type	Nominal radius (μm)	Gauge length (mm)	Temperature range (°C)	Stress range (MPa)	Atmosphere	Stress exponent, n	Reference
Tyranno® SA (SiC)	5	25/100	1400	<500	air	2	[4]
Tyranno® SA (SiC)	5	115	1400	<500	Ar	2	[4]
Nicalon™ (Si-C-O)	8	78	1000–1300	50–800	air	0.97–1.9	[5]
Nicalon™ (Si-C-O)	8	78	1000–1300	50–800	Ar	0.97–1.9	[5]
Nicalon™ (Si-C-O)	8	34–38	1200–1300	150–700	CO, CO/Ar	0.99	[6]
Hi-Nicalon™ (Si-C-O)	7	110	1180–1400	150–700	air	1.87–3.04	[7]
Hi-Nicalon™ (Si-C-O)	7	30–37	1300–1400	300–700	Ar	1.9–3.3	[7]
Hi-Nicalon™ (SiC)	6.5	25/100	1400	<500	air	1	[4]
Hi-Nicalon™ S (SiC)	6.5	115	1400	<500	Ar	1	[4]
Sylramic™ (SiC)	5	25/100	1400	<500	air	2	[4]
Sylramic™ (SiC)	5	115	1400	<500	Ar	2	[4]

TABLE II Fibre radius variation data for ceramic fibres based on the silicon carbide system [16–19]

Fibre type	Investigated fibre length, $2L$ (mm)	Mean radius, $r_{o\,(}$ μm)	Minimum/ maximum radius (μm)	Fractional radius variation, r_v	Radius variation wavelength, λ (mm)	Reference
Tyranno® LoxM (Si-C-O)	–	4.03	2.13/5.72	0.45	–	[16]
Tyranno® ZMI (Si-C-O)	500	5.5	2.78/7.22	0.40	130	[17]
Tyranno® SA (Si-C-O)	300	4.7	2.7/7.05	0.46	160	[18]
Nicalon™ (Si-C-O)	–	8.0	4/11	0.44	–	[19]
Hi-Nicalon™ (Si-C-O)	250	6.9	3.9/10.1	0.45	160	[18]
Hi-Nicalon™ S (Si-C-O)	300	6.15	4.3/7.3	0.24	–	[18]
Sylramic™ (SiC)	300	4.6	3.1/7.45	0.47	–	[18]

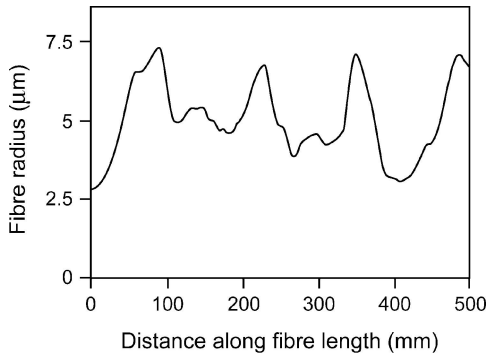

Figure 1 Variation of radius along the length of a Tyranno® ZMI Si-Zr-C-O fibre indicating the presence of a characteristic radius variation wavelength ($r_v \approx 0.4$, $\lambda \approx 130$ mm) [17].

approximate range $0.25 < r_v < 0.5$ and, furthermore, the radius often exhibits an approximate sinusoidal variation about the mean radius value with a characteristic radius variation wavelength, λ. Radius variation data for several SiC-based fibres have been presented in Table II [16–19]. The existence of a characteristic radius variation wavelength can be clearly seen in Fig. 1 for the case of Tyranno® ZMI Si-Zr-C-O fibres (Ube Industries Ltd., Ube City, Japan) with r_v and λ estimated to be 0.4 and 130 mm, respectively [17].

Whilst the creep rate of ceramic fibre bundles containing fibres with different radii has already been treated [20], the effect of variable fibre radius on $\dot{\varepsilon}$ for individual fibres is still unknown. Clearly, the existence of such large variations in current SiC-based fibres raises at least the possibility of this being a cause of significant error in the measurement of $\dot{\varepsilon}$. The present work will thus investigate the effect of fibre radius variation on creep rate for fibres with different radius variation geometries. The aim of this investigation is to determine whether fibre radius variation has any significant effect on the estimation of $\dot{\varepsilon}$ and, if so, what are the main factors that control the error in $\dot{\varepsilon}$.

2. Experimental procedure

Fibre radius geometries investigated in the present work have been presented in Fig. 2 with all geometries being considered to comprise of a sinusoidal radius variation superimposed onto a mean radius value. The linear variation (LV) and sinusoidal variation (SV) geometries would be expected to approximate the creep response of fibres at very small, i.e., $2L \ll \lambda$, and very large, i.e., $2L \gg \lambda$, gauge lengths, respectively. In contrast to this, the partial sinusoidal variation geometries (PSV-A, PSV-B, PSV-C) would approximate the creep response of fibres at intermediate gauge lengths, i.e., $2L \cong \lambda$, with each of the geometries differing only by the phase, ϕ, of the sinusoidal radius variation at the fibre mid-point; $\phi = 0$ (PSV-A), $\phi = \pi/2$ (PSV-B), and $\phi = -\pi/2$ (PSV-C). In addition to fibre geometry, the effect of varying n ($0 < n < 3$) and r_v ($0 < r_v < 0.5$) was also investigated with the ranges of n and r_v being similar to those of current SiC-based fibres (Tables I and II).

The fibre radius, and hence σ, at any point, x, along the fibre ($-L < x < L$) may be simply deduced for each of the geometries. For example, the fibre radius and stress for the LV geometry would be given by:

$$r(x)_{LV} = r_o\left(1 + \frac{r_v}{L}x\right) \tag{2}$$

and

$$\sigma(x)_{LV} = \frac{F}{\pi r_o^2}\frac{1}{\left(1 + \frac{r_v}{L}x\right)^2} \tag{3}$$

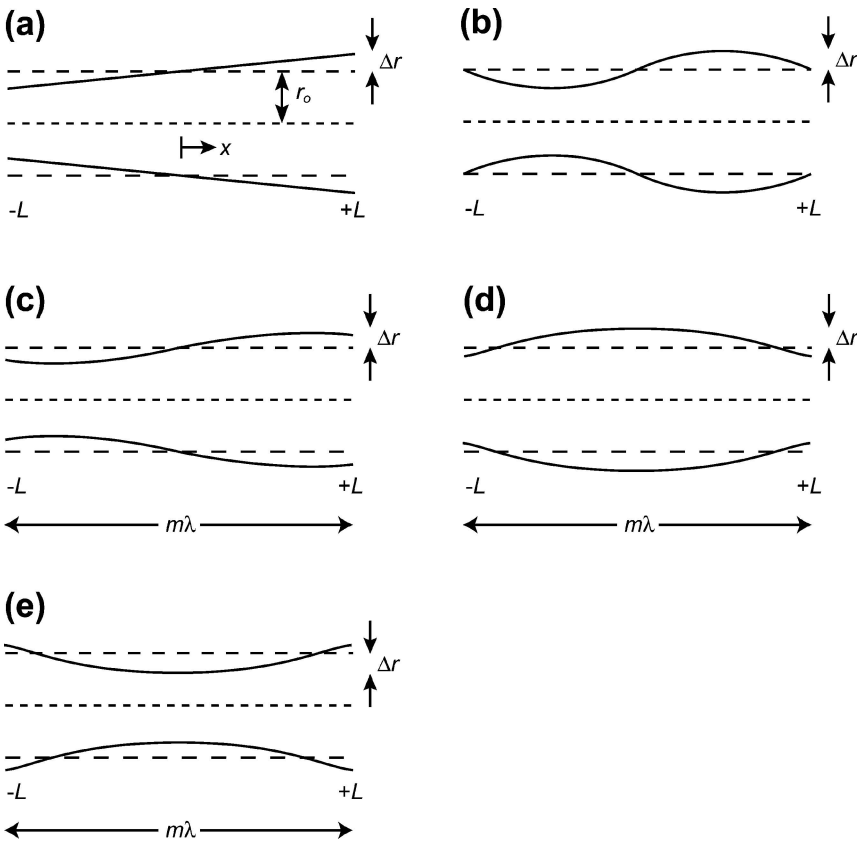

Figure 2 Fibre radius geometries used in the present work: (a) linear variation (LV), (b) sinusoidal variation (SV), (c) partial sinusoidal variation A (PSV-A), (d) partial sinusoidal variation B (PSV-B), and (e) partial sinusoidal variation C (PSV-C).

The creep rate, $\dot{\varepsilon}(x)$, at any position along the fibre can then be calculated from Equation (1), e.g.,

$$\dot{\varepsilon}(x)_{LV} = \frac{AF^n e^{-\left(\frac{Q}{RT}\right)}}{\pi^n r_o^{2n}} \left(1 + \frac{r_v}{L}x\right)^{-2n} \tag{4}$$

whilst the total creep rate for the fibre, $\dot{\varepsilon}$, would be given by integrating $\dot{\varepsilon}(x)$ along the fibre length, e.g.,

$$\dot{\varepsilon}_{LV} = \frac{AF^n e^{-\left(\frac{Q}{RT}\right)}}{\pi^n r_o^{2n}} \int_{-L}^{+L} \left(1 + \frac{r_v}{L}x\right)^{-2n} dx \tag{5}$$

The calculated creep rates were then normalised with respect to a fibre with $\Delta r = 0$, i.e., constant radius, with the normalised creep rate, $\dot{\varepsilon}^*$, for the LV geometry being given by:

$$\dot{\varepsilon}^*_{LV} = \frac{1}{2L} \int_{-L}^{+L} \left(1 + \frac{r_v}{L}x\right)^{-2n} dx \tag{6}$$

The respective equation for the SV geometry would be:

$$\dot{\varepsilon}^*_{SV} = \frac{1}{2L} \int_{-L}^{+L} \left(1 + r_v \sin\left(\frac{\pi}{L}x\right)\right)^{-2n} dx \tag{7}$$

Expressions for the different $\dot{\varepsilon}^*$ values as a function of r_v can be solved analytically for the special case of $n = \{0, \frac{1}{2}, 1, \frac{3}{2}, \ldots z\}$ with analytical solutions for $\dot{\varepsilon}^*_{LV}$ and $\dot{\varepsilon}^*_{SV}$ being presented in Table III for the case of $n = \{0, \frac{1}{2}, 1, \ldots 3\}$. However, it is not possible to analytically solve $\dot{\varepsilon}^*$ for the general case of n and thus a numerical method must be utilised.

Therefore, the creep rate for each set of conditions was calculated by dividing the fibre into 10^6 equal divisions along its length, calculating the creep rate for each of the divisions, and numerically integrating the result; the value of 10^6 divisions had been arrived at in preliminary calculations as a suitable comprise between accuracy and speed. It should be noted that, for significant creep lifetimes, it might be imagined that the fibre cross-section would decrease due to the increas-

TABLE III Analytical solutions for the normalised creep rate of the linear variation (LV) and sinusoidal variation (SV) geometries as a function of stress exponent

	Normalised creep rate, $\dot{\varepsilon}^*$	
Stress exponent, n	Linear variation (LV) geometry	Sinusoidal variation (SV) geometry
0	1	1
$\frac{1}{2}$	$\frac{\tanh^{-1}(r_v)}{r_v}$	$\frac{1}{\sqrt{1-r_v^2}}$
1	$\frac{1}{1-r_v^2}$	$\frac{1}{(1-r_v^2)^{3/2}}$
1 $\frac{1}{2}$	$\frac{1}{(1-r_v^2)^2}$	$\frac{r_v^2+2}{2(1-r_v^2)^{5/2}}$
2	$\frac{r_v^2+3}{3(1-r_v^2)^3}$	$\frac{3r_v^2+2}{2(1-r_v^2)^{7/2}}$
2 $\frac{1}{2}$	$\frac{r_v^2+1}{(1-r_v^2)^4}$	$\frac{3r_v^4+24r_v^2+8}{8(1-r_v^2)^{9/2}}$
3	$\frac{r_v^4+10r_v^2+5}{5(1-r_v^2)^5}$	$\frac{15r_v^4+40r_v^2+8}{8(1-r_v^2)^{11/2}}$

ing creep strain (with the result that the fibre creep rate would increase further) and thus the data presented within this investigation refers only to the initial creep rate.

3. Results and discussion

3.1. Linear and sinusoidal geometries

Values of normalised initial creep rate, $\dot{\varepsilon}^*$, for the LV and SV geometries have been presented in Fig. 3a and b, respectively, for the region $0 < n < 3$ and $0 < r_v < 0.5$. The numerical solutions for $\dot{\varepsilon}^*_{LV}$ and $\dot{\varepsilon}^*_{SV}$ obtained using $n = \{0, \frac{1}{2}, 1, \ldots 3\}$ and $0 < r_v < 0.5$ were found to be almost identical (typically within 0.001%) to those obtained analytically from Table III, thus confirming the validity of the numerical method employed. In both Fig. 3a and b it is clear that $\dot{\varepsilon}^*$ increases with n and r_v with, for example, $\dot{\varepsilon}^*_{LV} = 1.33$ for the case of $n = 1$ and $r_v = 0.5$, i.e., the initial creep rate would be 33% greater compared to that of a constant radius fibre with the same mean radius. The equivalent value for $\dot{\varepsilon}^*_{SV}$ (Fig. 3b) was 1.54, indicating the potential for large geometrical effects on the measured creep rate of current ceramic fibres. It can also be seen from Fig. 3 that $\dot{\varepsilon}^*_{SV} > \dot{\varepsilon}^*_{LV}$, implying that geometrical effects play a more significant role for creep measurements involving fibres with long gauge lengths, i.e., $2L \gg \lambda$, which can be inferred to be on the order of several hundred millimetres for the SiC-based fibres mentioned in Table II. Whilst it can be seen from Table I that, in practice, the maximum fibre gauge lengths tend to be on the order of $2L \approx \lambda$, the issue mentioned above may become of concern should future ceramic fibres be developed with smaller λ values. Another point of interest that can be deduced from $\dot{\varepsilon}^*_{SV} > \dot{\varepsilon}^*_{LV}$ is that, from the point of view of reducing the influence of radius variation and given the choice of LV and SV geometries, it would be preferable to use the smallest gauge length possible, i.e., $2L \ll \lambda$, in order to approximate the LV geometry. Indeed, this would also make sense from another point of view as the magnitude of the radius variation would necessarily be smaller for $2L \ll \lambda$ compared to $2L \geq \lambda$. However, the experimental difficulties associated with measuring ceramic fibre creep rates would suggest fibre gauge lengths to have a practical lower limit below which experimental errors increase significantly.

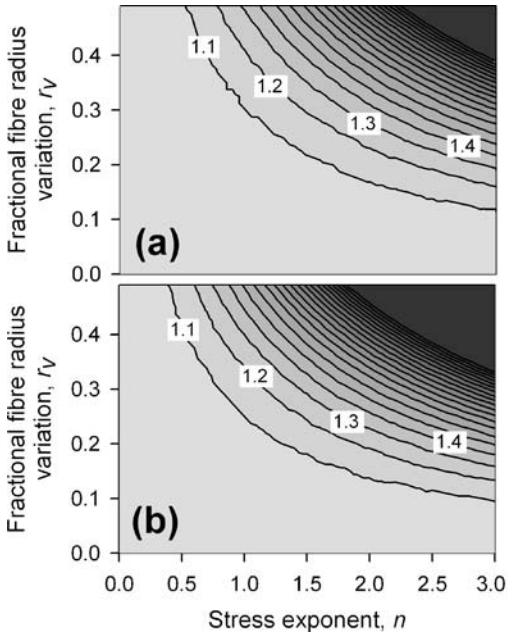

Figure 3 Normalised initial creep rate as a function of fractional fibre radius variation and creep stress exponent: (a) linear variation (LV) geometry, and (b) sinusoidal variation (SV) geometry.

The normalised initial creep rate for $r_v = 0.5$ was found to increase significantly to 2.57 ($\dot{\varepsilon}^*_{LV}$) and 3.76 ($\dot{\varepsilon}^*_{SV}$) for $n = 2$ and then to 6.37 ($\dot{\varepsilon}^*_{LV}$) and 11.52 ($\dot{\varepsilon}^*_{SV}$) for $n = 3$, which is well within the range of n for current SiC-based fibres. Such high values of $\dot{\varepsilon}^*$ for the LV and SV geometries again strongly suggest that geometrical variations within ceramic fibres may greatly influence experimentally measured creep rates.

Regarding the effect of relatively minor radius variations on $\dot{\varepsilon}^*_{LV}$ and $\dot{\varepsilon}^*_{SV}$ (with $n = 3$), Fig. 3 indicates the maximum allowable value of r_v for an error of 5% in $\dot{\varepsilon}^*$ (compared to the constant radius case) to be 0.083 ($\dot{\varepsilon}^*_{LV}$) and 0.068 ($\dot{\varepsilon}^*_{SV}$) whilst the respective values for a 10% error would be 0.116 and 0.095. From these results it is clear that even small variations in fibre radius (on the order of 5–10%) may have a noticeable effect on $\dot{\varepsilon}^*$ and it is thus suggested that the presence of any variation in fibre radius should be accurately determined for all ceramic fibres undergoing monofilament creep testing.

3.2. Partial sinusoidal geometries

The effect of stress exponent on initial creep rate for the partial sinusoidal geometries was investigated for the range $0 < m < 3$, where m is the characteristic wavelength fraction and $m = 2L/\lambda$. The value of r_v was kept constant at 0.5 for all cases in order to represent the maximum radius variation likely to be encountered with current ceramic fibres, and thus the values presented in this section will tend to indicate the upper limit of $\dot{\varepsilon}^*$.

The initial part of this investigation considered the range $0 < m < 0.5$, corresponding to $2L \leq \lambda/2$, with results being presented in Fig. 4. The first point of interest concerned the relative order of $\dot{\varepsilon}^*$ with $\dot{\varepsilon}^*_{PSV-A} >> \dot{\varepsilon}^*_{PSV-C} > \dot{\varepsilon}^*_{PSV-B}$. For example, the case of $n = 1$ and $m = 0.5$ gave values of 1.54 ($\dot{\varepsilon}^*_{PSV-A}$), 1.05 ($\dot{\varepsilon}^*_{PSV-B}$), and 1.15 ($\dot{\varepsilon}^*_{PSV-C}$) with the respective values for $n = 2$ and 3 being 3.76, 1.17, 1.54 and 11.52, 1.40, 2.29; indicating the difference between the $\dot{\varepsilon}^*_{PSV-A}$ and $\dot{\varepsilon}^*_{PSV-B}$, $\dot{\varepsilon}^*_{PSV-C}$ values to increase rapidly with n. It is also clear from Fig. 4 that the PSV-B and PSV-C geometries, unlike PSV-A, allow the use of relatively large gauge lengths with only a minor increase in $\dot{\varepsilon}^*$. For example, m values up to 0.34 (PSV-B) result in less than a 1% increase in $\dot{\varepsilon}^*$ for $n = 1$ with the upper limit for m being 0.20 for $n = 3$. The respective values for the PSV-C geometry were 0.21 and 0.12. Therefore, it is concluded to be extremely important to note the sinusoidal phase of the radius variation at the fibre midpoint for gauge lengths less than $\lambda/2$. Furthermore, the

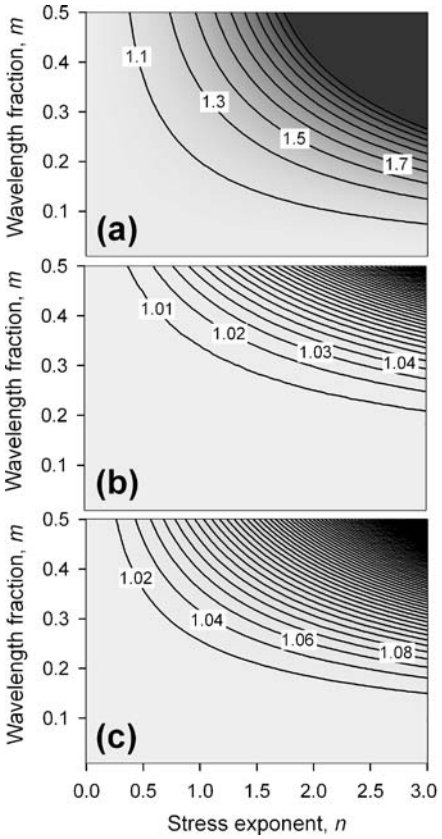

Figure 4 Normalised initial creep rate as a function of wavelength fraction ($0 < m < 0.5$) for $r_v = 0.5$: (a) partial sinusoidal variation A (PSV-A), (b) partial sinusoidal variation B (PSV-B), and (c) partial sinusoidal variation C (PSV-C).

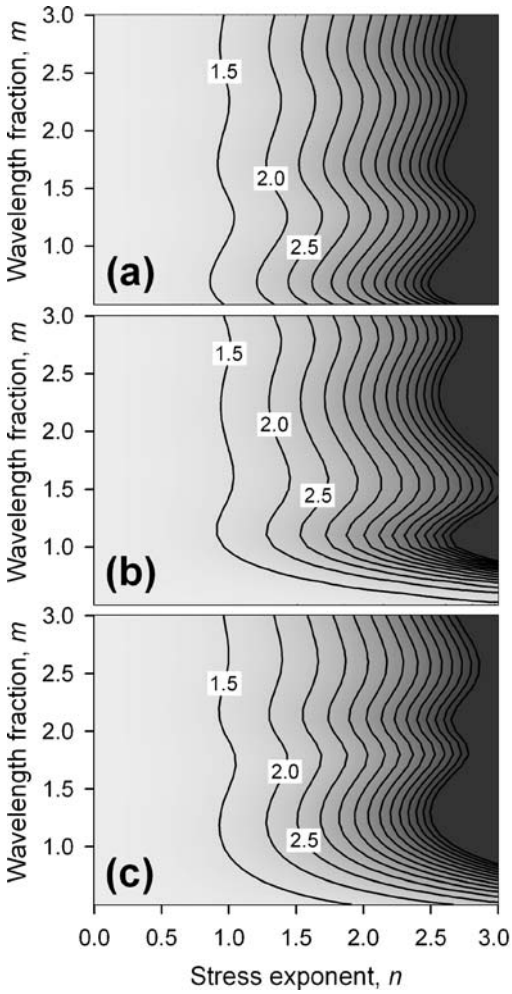

Figure 5 Normalised initial creep rate as a function of wavelength fraction ($0.5 < m < 3$) for $r_v = 0.5$: (a) partial sinusoidal variation A (PSV-A), (b) partial sinusoidal variation B (PSV-B), and (c) partial sinusoidal variation C (PSV-C).

main result of this work is that, from comparing Fig. 3 and 4, values of $\dot{\varepsilon}^*$ closest to unity are achieved through using the PSV-B geometry (closely followed by PSV-C) and small m, i.e., it is recommended that, from the point of view of fibre radius variability, ceramic fibre creep measurements should be carried out on fibres: (i) where the radius has an extreme value (preferably a maximum) at the fibre mid-point, and (ii) utilising the smallest practicable gauge length.

From comparison between Fig. 3 and 4 it is clear that the general magnitude and trend of the $\dot{\varepsilon}^*_{PSV-A}$ data (Fig. 3a) is similar to that of $\dot{\varepsilon}^*_{LV}$ (Fig. 4a) and $\dot{\varepsilon}^*_{SV}$ (Fig. 4b). Such a trend would be expected as it can easily be shown that $\dot{\varepsilon}^*_{PSV-A} \cong \dot{\varepsilon}^*_{LV}$ for $2L \rightarrow 0$ and $\dot{\varepsilon}^*_{PSV-A} = \dot{\varepsilon}^*_{SV}$ for $2L = \lambda/2$, i.e., the LV and SV geometries lie at either end of the $0 < m < 0.5$ range for the $\dot{\varepsilon}^*_{PSV-A}$ geometry.

The effect of stress exponent on $\dot{\varepsilon}^*$ for the range $0.5 < m < 3$ has been presented in Fig. 5 for the partial sinusoidal geometries with it being apparent that $\dot{\varepsilon}^*_{PSV-A} \cong \dot{\varepsilon}^*_{PSV-B} \cong \dot{\varepsilon}^*_{PSV-C}$ for $m \geq 1$. This result suggests that, as the gauge length becomes larger than the radius variation wavelength, i.e., $2L \geq \lambda$, then the relative phase of the radius variation at the fibre mid-point becomes less important with the error in this assumption being quantified later, i.e., $\dot{\varepsilon}^*$ can be estimated with knowledge only of r_v and n. However, it should be borne in mind that the $\dot{\varepsilon}^*$ values shown in Fig. 5 were generally larger compared to those in Fig. 4 (particularly for PSV-B and PSV-C), indicating that a reduction in gauge lengths would still be the preferred option.

The effect of m and r_v on $\dot{\varepsilon}^*$ for the case of $n = 2$ has been presented in Fig. 6 with the oscillations in $\dot{\varepsilon}^*$ data (about the respective $\dot{\varepsilon}^*_{SV}$ values) for $m \geq 1$ being significantly reduced for $r_v \leq 0.3$, suggesting $\dot{\varepsilon}^*$ to be relatively independent of m in the range $m \geq 1$ when $r_v \leq 0.3$. Indeed, the magnitude of the oscillations in the $\dot{\varepsilon}^*$ data within this region ($m \geq 1$, $r_v \leq 0.3$) was less than $\pm 5\%$ of the mean value. However, for the $r_v = 0.4$ and 0.5 cases the oscillations were increasingly significant and on the order of $\pm 12\%$ for $1 < m < 2$ and gradually decayed with increasing m to reach a value of $\pm 4\%$ for $m \cong 5$. The physical basis for the oscillation in $\dot{\varepsilon}^*$ data is attributed to the presence of gauge lengths containing non-integer multiples of λ as can be evidenced by the oscillation wavelengths being on the order of λ. The relative influence of the fractional values of λ became diminished as m increased and hence the oscillations in $\dot{\varepsilon}^*$ data decayed asymptotically towards $\dot{\varepsilon}^*_{SV}$ for $m \rightarrow \infty$. Therefore, for fibres with large radius variations, e.g., $r_v > 0.3$, unless an error of up to 12% in the value of $\dot{\varepsilon}^*$ is acceptable then it is necessary to know the phase of the radius variation at the fibre mid-point even for relatively large gauge lengths.

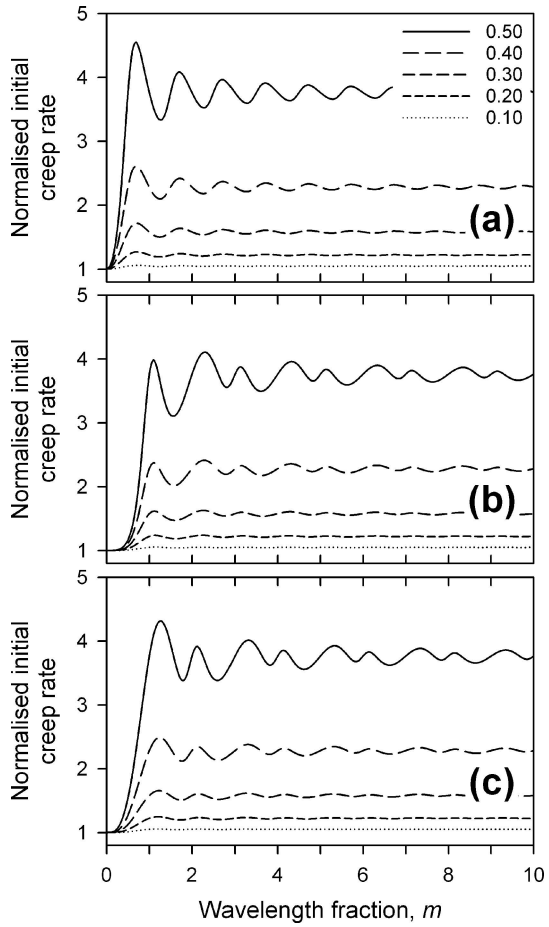

Figure 6 Effect of wavelength fraction and fractional radius variation on normalised initial creep rate for $n = 2$: (a) partial sinusoidal variation A (PSV-A), (b) partial sinusoidal variation B (PSV-B), and (c) partial sinusoidal variation C (PSV-C).

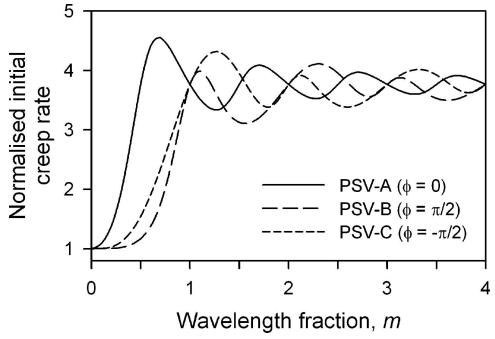

Figure 7 Comparison between normalised initial creep rates ($n = 2$; $r_v = 0.50$) for the different partial sinusoidal geometries at small $2L/\lambda$ ratios.

A comparison illustrating the difference in $\dot{\varepsilon}^*$ for the different partial sinusoidal geometries at small $2L/\lambda$ ratios and $r_v = 0.5$ has been presented in Fig. 7. It is clear for these geometries that $\dot{\varepsilon}^*$ changed significantly between $0 < m < 1$ with the initial (and maximum) peak $\dot{\varepsilon}^*$ values occurring at m values of 0.7 ($\dot{\varepsilon}^*_{PSV-A}$), 1.1 ($\dot{\varepsilon}^*_{PSV-B}$), and 1.3 ($\dot{\varepsilon}^*_{PSV-C}$). The rapidly varying and out of phase nature of the $\dot{\varepsilon}^*$ values within this region would again confirm the need to take into account the fibre geometry when measuring the creep of large radius variation ceramic fibres with gauge lengths on the order of λ.

4. Conclusions

The influence of radius variation on the normalised initial creep rate, $\dot{\varepsilon}^*$, of monofilament fibres was investigated using a numerical integration method. Five radius variation geometries, i.e., LV, SV, PSV-A, PSV-B, and PSV-C, were analysed in addition to the effects of varying the creep stress exponent, n, fractional radius variation, r_v, and the fraction, m, of the radius variation characteristic wavelength, λ. The range of n and r_v under investigation (i.e., $0 < n < 3$, $0 < r_v < 0.5$) was chosen as being representative of current ceramic fibres based on the silicon carbide system. The major conclusions from this study were:

(i) The value of $\dot{\varepsilon}^*$ was always found to be greater compared to that of a constant radius fibre with the same mean radius, r_o, indicating that the presence of radius variations within monofilament fibre creep specimens will always increase the measured creep rate above the intrinsic material-related value.

(ii) When comparing the LV and SV geometries it was noted that $\dot{\varepsilon}^*_{SV} > \dot{\varepsilon}^*_{LV}$ whilst $\dot{\varepsilon}^*$ increased with both n and r_v. For the case of $r_v = 0.5$ it was found that $\dot{\varepsilon}^*_{LV}$ had values of 1.33, 2.57, and 6.37 for $n = 1, 2$, and 3, respectively, and raised the possibility of radius variation within ceramic fibres playing an important role in the measurement of creep rates. Even relatively small radius variations ($r_v = 5$–10%) were found to result in increases on the order of 5% for $\dot{\varepsilon}^*$.

(iii) Comparing PSV geometries in the range $0 < m < 0.5$ indicated $\dot{\varepsilon}^*$ to be generally smaller compared to that of the LV and SV geometries, particularly for the PSV-B geometry where the radius was maximum at the fibre mid-point (and closely followed by the PSV-C geometry). For the case of $n = 3$ it was found that gauge lengths of up to $\lambda/5$ resulted in $\dot{\varepsilon}^*_{PSV-B}$ being within 1% of the constant radius value. PSV geometries in the range $0.5 < m < 3$ exhibited oscillations in the $\dot{\varepsilon}^*$ data that decayed asymptotically with increasing m towards the respective $\dot{\varepsilon}^*_{SV}$ value.

(iv) The main conclusion of this work is the recommendation that creep testing of monofilament ceramic fibres should be limited to fibres where the radius variation is symmetrical and exhibits a maximum value at the fibre mid-point and that gauge lengths should be as small as practically possible, e.g., $\lambda \leq /5$, which corresponds to an approximate upper limit of 26–32 mm for current SiC-based fibres.

Acknowledgements

The author gratefully acknowledges Tetsuya Morimoto of the Japan Aerospace Exploration Agency (JAXA) for his useful comments and suggestions concerning this investigation.

References

1. H. OHNABE, S. MASAKI, M. ONOZUKA, K. MIYAHARA and T. SASA, *Composites: Part A* **30** (1999) 489.
2. H. G. HALVERSON and W. A. CURTIN, *J. Am. Ceram. Soc.* **85(6)** (2002) 1350.
3. J. E. DORN, *J. Mech. Phys. Solids.* **3** (1954) 85.

4. H. M. YUN and J. A. DICARLO, *Ceram, Eng. Sci. Proc.* **20**(**3**) (1999) 259.
5. G. SIMON and A. R. BUNSELL, *J. Maters. Sci.* **19** (1984) 3658.
6. R. BODET, J. LAMON, N. JIA and R. E. TRESSLER, *J. Am. Ceram. Soc.* **79**(**10**) (1996) 2673.
7. R. BODET, X. BOURRAT, J. LAMON and R. NASLAIN, *J. Maters. Sci.* **30** (1995) 661.
8. D. M. WILSON, *J. Maters. Sci.* **32** (1997) 2535.
9. E. LARA-CURZIO and C. M. RUSS, *J. Maters. Sci. Letts.* **18** (1999) 2041.
10. T. MORIMOTO, *Int. J. Maters. Prod. Technol.* **16**(**1–3**) (2001) 22.
11. I. J. DAVIES, *J. Maters. Sci. Letts.* **20**(**12**) (2001) 1103.
12. I. J. DAVIES and T. ISHIKAWA, *J. Maters. Sci. Letts.* **20**(**6**) (2001) 505.
13. T. A. PARTHASARATHY, *J. Am. Ceram. Soc.* **84**(**3**) (2001) 588.
14. Y. ZHANG, X. WANG, N. PAN and R. POSTLE, *J. Maters. Sci.* **37** (2002) 1401.
15. T. MORIMOTO, *Composites: Part A* **34** (2003) 597.
16. I. J. DAVIES, T. ISHIKAWA, M. SHIBUYA, T. HIROKAWA and J. GOTOH, *Composites: Part A* **30** (1999) 587.
17. T. MORIMOTO, in Proceedings of the 9th US-Japan conference on composite materials, Mishima, Japan, July 2000, edited by H. Fukuda, T. Ishikawa, and Y. Kogo (Japan society for composite materials, Tokyo, Japan, 2000) p. 265.
18. G. E. YOUNGBLOOD, C. R. EIHOLZER, C. A. LEWINSOHN, R. H. JONES, A. HASEGAWA and A. KOHYAMA, *Ceram. Eng. Sci. Proc.* **20**(**3**) (1999) 481.
19. Y. T. ZHU, S. T. TAYLOR, M. G. STOUT, D. P. BUTT, W. R. BLUMENTHAL and T. C. LOWE, *ibid.* **18**(**3**) (1997) 119.
20. F. MACDONALD and D. COON, *J. Maters. Sci.* **36** (2001) 1681.

Received 2 April 2004
and accepted 9 May 2005